

Spatially patterned static roughness superimposed on thermal roughness in a condensed phospholipid monolayer

W. R. Schief,¹ S. B. Hall,² and V. Vogel^{3,*}

¹*Department of Physics, University of Washington, Seattle, Washington 98195*

²*Department of Biochemistry and Molecular Biology, Department of Medicine, and Department of Physiology and Pharmacology, Oregon Health Sciences University, Portland, Oregon 97201*

³*Department of Bioengineering and Department of Physics, University of Washington, Seattle, Washington 98195*

(Received 16 August 1999; revised manuscript received 7 July 2000)

Imaging of diffuse light scattering in reflection from a phospholipid monolayer at the air/water interface has revealed a previously undetected separation of the monolayer into two regions distinguishable by the intensity of their scattering. In monolayers of *L*-dipalmitoyl phosphatidylcholine in the condensed phase, chiral-shaped domains are surrounded by a brighter region that covers approximately half the monolayer. While the scattered intensity from both regions increases with surface pressure in a manner consistent with scattering from thermally induced capillary waves, the additional scattering from the brighter region indicates a static surface roughness superimposed on the thermal roughness.

PACS number(s): 68.55.-a, 68.10.Cr, 68.35.Ct, 87.64.Cc

I. INTRODUCTION

Light scattering from thermally roughened fluid interfaces has served as a tool for the study of critical phenomena at two-phase boundaries, surface adsorption processes, and interfacial properties of molecular monolayers [1]. Probing interfaces with scattering techniques allows remote study, and thereby minimizes perturbations. Till now, scattering techniques based on light, x rays, or neutrons have not provided information on surface heterogeneity at fluid interfaces on length scales below the diameter or coherence of the incident beam. In this paper, the imaging of diffuse light scattering reflected from a monolayer-covered air/water interface not only detects the presence of thermally excited capillary waves with amplitudes smaller than 10 Å, but also reveals a previously undetected, microscopically patterned, static surface roughness that is overlaid on the thermal roughness.

Related to dark field microscopy [2], our implementation of light scattering microscopy (LSM) forms an image of the monolayer by illuminating the interface with a laser at an oblique angle and collecting scattered light distributed about the surface normal in reflection (Fig. 1). In this work the laser beam is *p* polarized and incident at Brewster's angle for the bare interface ($\theta_B = \tan^{-1}[n_{\text{water}}/n_{\text{air}}]$) so the monolayer specular reflectivity can be imaged simultaneously with Brewster angle microscopy [3] (BAM). These particular conditions chosen to allow BAM are not necessary for high sensitivity to monolayer scattering with LSM.

LSM is employed here to probe the nanoscale topography of monolayers of the chiral lipid *L*-dipalmitoyl phosphatidylcholine (*L*-DPPC) at the air/water interface. *L*-DPPC monolayers are prevalent in the study of two-dimensional (2D) phase transitions, and are thought to play a crucial role in the function of lung surfactant films. At temperatures above the

triple point, isothermal compression of single component lipid monolayers typically produces a sequence of 2D phases proceeding with increasing density from gas (*G*)→liquid-expanded (LE)→tilted-condensed (TC)→untilted-condensed (UC) [4,5]. The TC and UC phases were previously labeled liquid-condensed and solid, respectively, but the new terminology more accurately reflects the state of polar tilt and correctly avoids suggesting a difference in translational order between the phases [4]. At the “collapse” pressure, lipid monolayers also show a variety of transitions into three dimensions [6]. For noncollapsed monolayers in the TC or UC phases at the air/water interface, no evidence to our knowledge has been reported for deviations from planarity, except for monolayer buckling under specialized conditions which confer unusually high compressional rigidity [7]. However, while TC domains grow in coexistence with the LE phase, the molecular orientations at the edges of adjacent TC domains are not aligned in general, so after disappearance of the LE phase a condensed film may contain an enhanced density of packing defects in the regions where TC domains grew together. Therefore, condensed lipid monolayers might yield into the third dimension at the boundaries between formerly distinct TC domains, at pressures below collapse. LSM was implemented to test this hypothesis. As described below, LSM reveals the emergence of a spatially

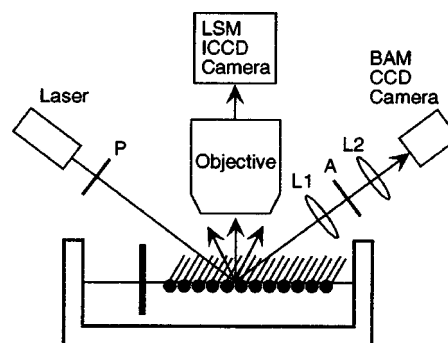


FIG. 1. Schematic of the LSM and BAM. For details, Sec. II.

*Author to whom correspondence should be addressed. Email address: vvogel@u.washington.edu

patterned increase in light scattering upon compression of L-DPPC monolayers into the TC phase. The region of increased scattering surrounds domains that scatter less light and possess chiral shapes characteristic of TC domains of L-DPPC. Analysis of the scattered intensities indicates that the chiral domains possess only thermal roughness, and that the increased scattering in the surrounding region results from either static topographic deformations of the monolayer or multilayer particles on the monolayer. These results show that the monolayer does indeed yield in the boundary regions of TC domains. As detailed elsewhere [8], the region of increased scattering promotes the formation of nanoscale protrusions normal to the surface (“buds”) upon compression to higher pressures, and these buds are precursors of monolayer collapse.

II. MATERIALS AND METHODS

A. Langmuir trough and solutions

L-DPPC (>99%, Avanti Polar Lipids, Sigma) was dissolved in chloroform (Sigma, HPLC grade, 99.9%) and spread on water (resistivity >18.0 M Ω , pH=5.6) or buffer (10-mM Hepes, 150-mM NaCl, 1.5-mM CaCl₂, pH=7.0) in a custom-built teflon trough (maximum area 532 cm²) with a continuous perimeter, vertical teflon ribbon (Labcon, Darlington, UK) to contain the film. Experiments at surface pressures below 40 mN/m were also reproduced using a smaller Langmuir trough with two moveable teflon barriers. All experiments were performed at room temperature (20°–22°), and continuous compression and expansion at a rate of (0.6 Å²/molecule)/min was employed. Buffer and salts were purchased from Sigma (SigmaUltra). The trough and microscopes rested on active electronic vibration isolation tables (Nanofilm Technologie, MOD 2).

B. Brewster angle microscopy (BAM)

A home-built Brewster angle microscope was mounted on the Langmuir trough (see Fig. 1). A laser beam of wavelength 532 nm (Coherent DPSS 532-100) set to *p* polarization

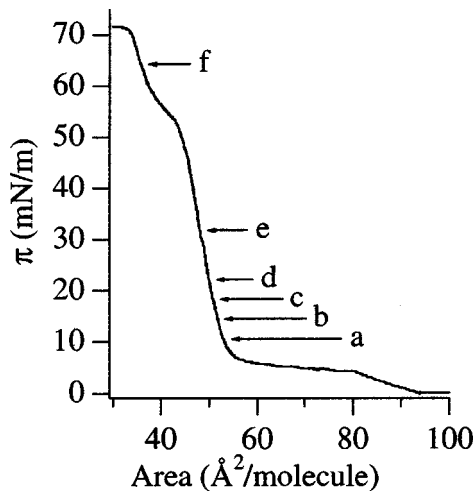


FIG. 2. π -*A* isotherm of L-DPPC on buffer at $T=22$ °C. Points labeled A–F correspond to the LSM images in Fig. 3.

tion with a Glan-Thompson polarizer (*P*) provided a power of ~ 90 mW incident on the air-buffer interface at Brewster’s angle ($\theta = \tan^{-1}(n_{\text{buffer}}/n_{\text{air}}) \approx 53.1^\circ$ from the surface normal). To obtain a coincident focus of the BAM and LSM required a long working distance in both microscopes. For BAM the reflected light was focused by a system of two single lenses (*L*₁ and *L*₂) with a working distance of ~ 65 mm through a Glan-Thompson analyzer (*A*) onto a CCD camera (Dage-MTI, CCD-72).

C. Light scattering microscopy (LSM)

LSM examined the same surface location as the BAM. Light from the BAM laser scattered about the surface normal was focused by an extra-long working distance objective (Nikon, *NA*=0.45, *WD*=9 mm) onto an image intensifier (Intevac Nitemate 1306) coupled to a CCD camera (Pulnix TM-745G). The linear responses of the camera alone and the intensifier-camera combination were verified in separate control experiments in which unpolarized light from a fiber optic light source passed through neutral density filter(s) and two

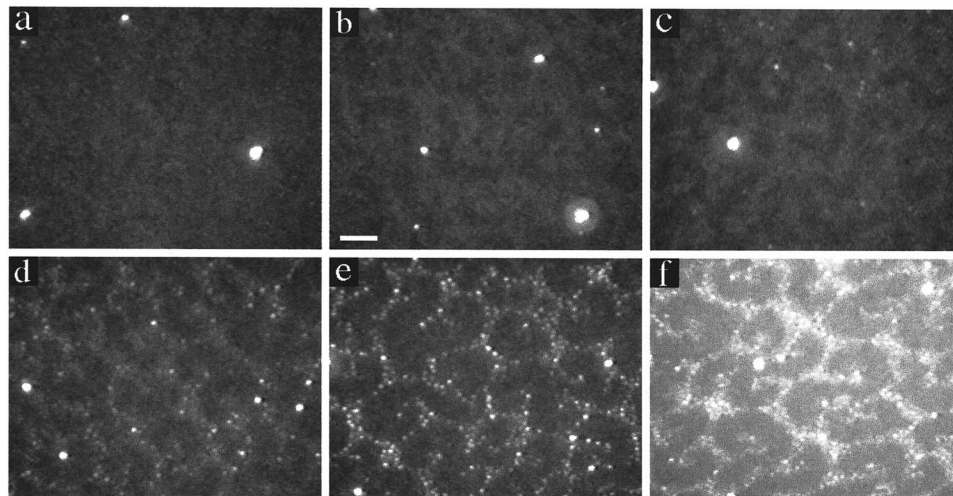


FIG. 3. LSM images of an L-DPPC monolayer on buffer recorded during compression. Images recorded at π (mN/m) of (a) 10.8, (b) 14.8, (c) 18.5, (d) 22.4, (e) 32.0, and (f) 64.4. The contrast in all six images has been enhanced identically to preserve the relative image intensities. The scale bar in (b) corresponds to 25 μm .



FIG. 4. LSM images of an L-DPPC monolayer on a buffer recorded during expansion following compression to a maximum pressure of $\pi = 40$ mN/m. Images recorded at π (mN/m) of (a) 17.0, (b) 14.5, and (c) 13.2. The contrast in all three images was enhanced identically to preserve the relative image intensities. The scale bar in (a) corresponds to $25 \mu\text{m}$.

polarizers, and illuminated a central portion of the detector. With camera gain settings similar to those used for detection of monolayer scattering, the mean image intensity extracted from the illuminated region of the detector varied linearly with the square of the cosine of the angle between the polarizer axes (the linear correlation coefficient is 0.998) throughout the range of gray scales investigated in this study.

III. RESULTS AND DISCUSSION

The surface pressure (π)–area isotherm for L-DPPC compressed slowly on buffer at $T = 22^\circ\text{C}$ is shown in Fig. 2. The prominent isotherm plateau at $\pi = 5$ mN/m indicates the first-order LE \rightarrow TC transition. In monolayers of the chiral lipid L-DPPC, the TC domains that grow from the LE phase display characteristic chiral shapes, linked to a twist of the in-plane orientation of the tilted hydrocarbon chains [9]. LSM resolves scattering from the edges of such TC domains while in coexistence with the LE phase, though the interiors of both the LE and TC phases appear dark [8]. The completion of the LE \rightarrow TC transition is observed at $\pi = 11 \pm 1$ mN/m, when the TC domains grow into a complete film and the LSM field becomes uniformly dark [Fig. 3(a)]. The few bright scattering points in Fig. 3(a) are nonlipid particles present at all surface pressures that do not impact significantly the phase behavior. Also at this pressure, BAM imaging confirms the disappearance of the LE phase and the appearance of long range chain tilt order across the entire monolayer (not shown).

After an area reduction of 1%, which raises the surface pressure from $\pi = 11$ to 13 mN/m, LSM reveals a previously undetected structural change in L-DPPC monolayers in the TC phase. Increased diffuse scattering appears in LSM in a continuous region covering approximately 55% [8] of the interface. The increased scattering persists for $\pi \geq 13 \pm 1$ mN/m, and can be visualized until $\pi = 60 \pm 1$ mN/m. Figures 3(b) and 3(c), recorded at $\pi = 14.8$ and 18.5 mN/m, respectively, are representative of the range $13 \leq \pi \leq 20$ mN/m. Although the monolayer previously converted to the TC phase (as discussed above), the region of increased scattering surrounds darker domains that possess the same range of chiral shapes as the TC domains grown during the LE \rightarrow TC transition. For example, Figs. 3(b) and 3(c) show the common “mirrored *s*” and “bean” shapes [10]. Both the dark domains and the surrounding region have spatially uniform brightness in LSM, with a current lateral resolution of $\sim 2.5 \mu\text{m}$. With the present sensitivity of the LSM, this separation of L-DPPC monolayers has been observed in ev-

ery one of at least 20 independent experiments on multiple high purity lipid samples from two suppliers. The findings are similar on water and buffer subphases, though on water the arms of the chiral domains are thinner and less resistant to deformation by flow anisotropy during compression. Control experiments with other lipid monolayers that do not reveal a separation of the film following the LE \rightarrow TC transition strongly indicate that the scattering contrast detected in L-DPPC monolayers is not due to the presence of impurities or some other systematic effect [8]. Consistent with previously measured isotherms of L-DPPC, there was no detectable change of compressibility in the isotherm (Fig. 2) at $\pi = 13$ mN/m.

At $\pi = 20 \pm 1$ mN/m, LSM reveals a second previously undetected structural change in L-DPPC monolayers in the TC phase. Bright point scatterers emerge within the region surrounding the chiral domains [Fig. 3(d)]. The number of point scatterers increases with pressure [Fig. 3(e)], and above $\pi = 60$ mN/m the scattering centers proliferate [Fig. 3(f)]. The point scatterers are stable at the air/water interface at constant or decreasing trough area: once formed, the individual scatterers are not observed to disappear unless the monolayer is expanded. Elsewhere [8], the point scatterers are shown to represent nanoscale bilayer and multibilayer particles (“buds”) which grow as protrusions from the monolayer and serve as precursors to monolayer collapse. In that work, a tapping-mode atomic force microscopy (AFM) analysis of L-DPPC films transferred to mica at surface pressures up to $\pi = 65$ mN/m shows that the point scatterers visible with LSM above $\pi = 20$ mN/m each correspond to one or more round particles spaced within the lateral resolution of the LSM with thicknesses generally in multiples of 4–6 nm and diameters of 15–150 nm. A significant number of point scatterers is not detected in the subphase, indicating that the buds may form above the monolayer. Evidently, the increased scattering surrounding the darker chiral domains for $\pi \geq 13$ mN/m reflects a structural change that leads to detectable nanoscale budding in the region surrounding the chiral domains at $\pi = 20$ mN/m.

Both the spatially patterned increase in scattering at $\pi = 13$ mN/m and the budding transition observed at $\pi = 20$ mN/m can be reversed by expansion of the monolayer. Figure 4 shows a sequence of three LSM images of an L-DPPC monolayer recorded during slow expansion after an initial compression to $\pi = 40$ mN/m. In Fig. 4(a), recorded at $\pi = 17$ mN/m during expansion, the monolayer has dark chiral domains surrounded by a region of increased scattering

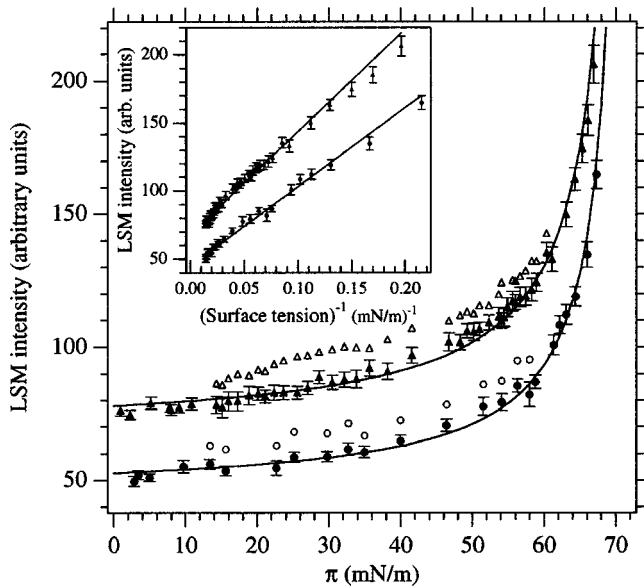


FIG. 5. LSM image intensities for the dark domains (filled symbols) and the surrounding region (open symbols) plotted vs π for two typical experiments (triangles and circles). The upper data (triangles) were taken with a higher camera gain. Intensities from both the LE and TC phases below $\pi=13$ mN/m are plotted as filled symbols. Each intensity represents the average of several measurements within the central, brightest region of a single image. Errors include the intensity variation within each image and the systematic effects discussed in the text. Errors are suppressed for the open symbols to facilitate visualization. The solid lines correspond to the least squares fits to $1/\gamma$ shown in the inset. Inset: intensities of the dark domains plotted vs $1/\gamma$ for the two experiments in the main graph, and the corresponding linear fits to $1/\gamma$.

that is spatially uniform, and the region of increased scattering is dotted with bright point scatterers corresponding to buds. After expansion to $\pi=14.5$ mN/m [Fig. 4(b)], the number of point scatterers per area has declined, but the contrast is still evident between the chiral domains and the brighter spatially uniform surrounding. Expansion to $\pi=13.2$ mN/m has caused the disappearance of the increased scattering surrounding the domains, leaving a uniform monolayer with a low density of point scatterers [Fig. 4(c)]. The remaining point scatterers, except for the brightest that correspond to nonlipid particles, reincorporate into the monolayer once the LE phase appears during further expansion (not shown). The reversibility of the increased scattering at $\pi=13$ mN/m has been reproduced with several L-DPPC monolayers that were initially compressed to $\pi < 20$ mN/m.

To investigate the physical origins of the diffuse scattering in the two regions that become distinguishable at $\pi=13$ mN/m—the chiral domains and the brighter surrounding region—an analysis of the pressure dependence of the LSM image intensities was employed. With a stable laser intensity ($\pm 3\%$ over 8 h), fixed camera gain and offset (a drift less than $\pm 1\%$), and a roughly constant water level (± 20 μm), intensities were extracted from both the domains and the surrounding region in the central, brightest part of the LSM images. The point scatterers that emerge in LSM above $\pi=20$ mN/m were excluded from intensity measurements in the surrounding region in order to monitor scatter-

ing due to structural features potentially distinct from bilayer and multilayer buds. Above $\pi=60$ mN/m, the proliferation of point scatterers within the surrounding region prevented intensity measurements there.

LSM intensities for both the domains (filled symbols) and the surrounding region (open symbols) are plotted versus π in Fig. 5 for two typical experiments (triangles and circles). The upper data (triangles) were taken with a higher camera gain. The solid lines correspond to fits of the domain intensities vs $1/\gamma$, where $\gamma=\gamma_0-\pi$ is the surface tension and $\gamma_0=72$ mN/m is the surface tension of the bare air/water interface. The inset of Fig. 5 shows directly the linear dependence on $1/\gamma$ of the domain intensities. The increased scattering in the surrounding region at $\pi=13$ mN/m and the parallel scaling of the intensities in the domains and the surrounding are evident in the main plot of Fig. 5. The intensities of both the domains and the surrounding region varied linearly with $1/\gamma$. Intensity analysis of three additional experiments agreed quantitatively.

The $1/\gamma$ scaling of the intensities is the signature of thermal roughness. According to capillary wave theory, if surface thermal roughness is described as a superimposition of sinusoidal modes with wavelength $\lambda_q=2\pi/q$ and amplitude ζ_q , the mean square amplitude of each mode scales as [11] $\langle \zeta_q^2 \rangle \propto 1/(\gamma q^2)$ within the range of surface wavelengths probed by LSM ($0.43 \leq \lambda_q \leq 1.52$ μm) [12]. A brief argument shows that the intensities measured by LSM due to thermal roughness should rise inversely in proportion to the surface tension ($I_{\text{LSM}} \propto 1/\gamma$) [13]. We conclude that, within the range of surface wavelengths probed by LSM, and within the sensitivity of the analysis (discussed below), the measured scattering from the chiral domains varies with surface tension as expected for thermal roughness and reveals no structural changes in the pressure range $0 \leq \pi \leq 67.3$ mN/m [14]. The domains are flat in a time-averaged sense. In addition, the $1/\gamma$ scaling of the intensity in the surrounding region indicates the presence of capillary waves outside the domains.

The physical origin of the increased scattering surrounding the domains for $\pi \geq 13$ mN/m remains to be determined. In principle, this uniform increase in light scattering over half the monolayer could be due to several possible sources: (1) spatial variations of in-plane molecular tilt orientation, (2) monolayer density variations, or (3) surface roughness. These light scattering sources potentially could be static or fluctuating in time. In addition, two or more of these sources could be superimposed or coupled. In the following subsections, we address the above possibilities.

A. In-plane molecular tilt variations

One possible source of the increased scattering at $\pi=13$ mN/m is a spatial variation of in-plane, or azimuthal, molecular orientation. Intuitively, this possibility is appealing since the splay across the curved arms of TC domains of L-DPPC [15,16] suggests that azimuthal tilt conflicts will arise between adjacent TC domains as they grow together. However, we find that scattering due to variations of in-plane tilt orientation in lipid monolayers is undetectable in LSM with the present sensitivity. In all of our studies of several lipids whose TC domains contain tilt azimuth “jumps” in

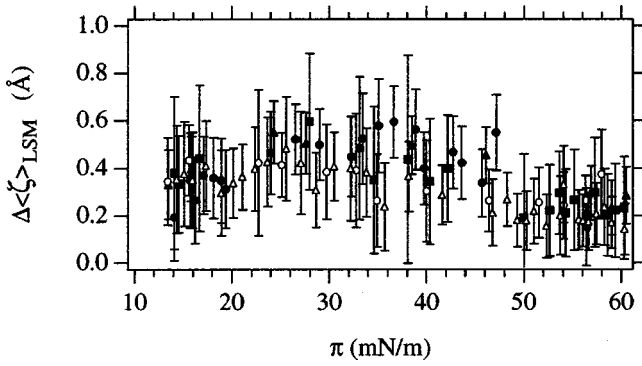


FIG. 6. Plot of $\Delta\langle\xi\rangle_{\text{LSM}}$ vs π . Different symbols denote data from five different experiments.

their interiors along boundaries visible with BAM, no detectable scattering from those boundaries has been found with LSM [17]. Furthermore, during the LE \rightarrow TC phase transition of L-DPPC, the scattered intensity in the interiors of TC domains is not measurably different from the intensity in the LE phase. The continuous variation of in-plane tilt orientation in the optically anisotropic TC domains of L-DPPC thus scatters no more strongly than an isotropic fluid phase. We conclude that spatial variations of in-plane molecular tilt orientation make a negligible contribution to the increased scattering at $\pi=13$ mN/m in L-DPPC monolayers, even though tilt orientation conflicts are likely present in the region of increased scattering.

B. Monolayer density inhomogeneity

In-plane density variations, either static or fluctuating, are another possible source of the increased scattering at $\pi=13$ mN/m. We now assess the strength of the scattering from monolayer density variations in comparison to the scattering from monolayer surface roughness. The comparison is made first for the case of thermal fluctuations and second for static spatial variations. Calculations [18] of the light intensity scattered from an isotropic monolayer by thermally excited capillary waves or 1D density fluctuations in the plane of incidence show that the intensity scattered by density fluctuations is smaller by a factor of $(\gamma/\varepsilon)(2\pi t/\lambda_q)^2 \sim 10^{-5}$ for nonresonantly polarizable films, where $t \sim 2$ nm is the monolayer thickness (assumed spatially invariant), $\lambda_q \sim 1$ μm is the wavelength of the variation, $\varepsilon \sim 200$ mN/m is the compressibility modulus, and $\gamma = 59$ mN/m at $\pi = 13$ mN/m. Thus thermally excited density fluctuations cannot be the source of the increased scattering. The calculations of Ref. [18] also allow a comparison of scattered intensities by static surface roughness and 1D spatial density variations of equal amplitude and wavelength, and show that scattering from static density variations is weaker by $(2\pi t/\lambda_q)^2 \sim 10^{-4}$. Therefore, density inhomogeneities cannot make a significant contribution to the increased scattering surrounding the domains at $\pi = 13$ mN/m.

C. Surface roughness

Having eliminated spatial variations in molecular tilt or monolayer density as origins of the increased scattering surrounding the chiral domains at $\pi = 13$ mN/m, we conclude

that the increase in scattering must be due to an increase in surface roughness. We now estimate the amplitude of the increased roughness in the region surrounding the chiral domains. The LSM intensity (I_{LSM}) is calibrated against $\langle\xi^2\rangle_{\text{LSM}}$, the mean square thermal roughness within the surface wavelengths probed by the LSM. $\langle\xi^2\rangle_{\text{LSM}} = \sum \langle\xi_q^2\rangle$, where $\langle\xi_q^2\rangle$ is the mean square surface displacement due to all fluctuations with spatial wave vector q , and the sum is carried from q_{min} to q_{max} corresponding to $0.43 \leq \lambda_q \leq 1.52$ μm . The calibration of I_{LSM} versus $\langle\xi^2\rangle_{\text{LSM}}$ is obtained by calculating $\langle\xi^2\rangle_{\text{LSM}}$ as a function of $1/\gamma$ from capillary wave theory, and then substituting for $1/\gamma$ using a fit of I_{LSM} versus $1/\gamma$ for the domains that possess thermal roughness only. The capillary wave model shows [19] that

$$\begin{aligned} \langle\xi^2\rangle_{\text{LSM}} &= (k_B T / 4\pi\gamma) \ln[1 + (Lq_{\text{max}})^2] / [1 + (Lq_{\text{min}})^2] \\ &\approx (k_B T / 4\pi\gamma) 2.55. \end{aligned} \quad (1)$$

Here T is the absolute temperature, $L^2 = \gamma / [(\rho_{\text{water}} - \rho_{\text{air}})g]$, and the approximate equality is accurate to within 1% for $\gamma \geq 10^{-3}$ mN/m. As an example, if we substitute for $1/\gamma$ in Eq. (1) using the fit of the lower data (filled circles) in Fig. 5 [$I_{\text{LSM}} = 44.6(\pm 0.7) + 583.4(\pm 14.9)/\gamma$, with I_{LSM} in arbitrary units and γ in mN/m], we obtain the calibration for that experiment: $I_{\text{LSM}} = 44.6(\pm 0.7) + 7.06(\pm 0.18)\langle\xi^2\rangle_{\text{LSM}}$ with $\langle\xi^2\rangle_{\text{LSM}}$ in \AA^2 . The sensitivity is remarkably high: from $\pi = 40$ to 67.3 mN/m, $\langle\xi\rangle_{\text{LSM}} = \sqrt{\langle\xi^2\rangle_{\text{LSM}}}$ rises from 1.6 to 4.2 \AA , an increase of 2.6 \AA , and the LSM intensity of the domains increases correspondingly by 106 units on a scale of 0–255.

The above calibration method provides an estimate for the amplitude of the additional roughness in the region surrounding the domains. From intensities extracted from L-DPPC monolayers in five separate experiments with different calibrations, we calculated the difference between the roughness in the region surrounding the domains and the roughness in the domains themselves ($\Delta\langle\xi\rangle_{\text{LSM}} = \langle\xi\rangle_{\text{LSM,SURR}} - \langle\xi\rangle_{\text{LSM,DOM}}$). Figure 6 shows a graph of $\Delta\langle\xi\rangle_{\text{LSM}}$ versus π . The data in Fig. 6 indicate that the surface roughness in the region surrounding the domains is 0.4 ± 0.2 \AA greater than the thermal roughness of the domains throughout the pressure range $13 \leq \pi < 50$ mN/m. This additional roughness declines to 0.2 \AA at $\pi = 50$ mN/m.

Are such small amplitudes physically reasonable? The small size of these amplitude estimates is physically plausible since they reflect only a narrow range of surface wavelengths. Equation (1) shows that the thermal roughness within the range of wavelengths probed by LSM is $\langle\xi\rangle_{\text{LSM}} = 1.2$ \AA at $\pi = 13$ mN/m and $T = 22^\circ\text{C}$, so an increase of 0.4 \AA represents a 30% growth in amplitude. Furthermore, we expect that increased roughness also occurs outside the surface wavelength range probed by LSM. Indeed, increased roughness at smaller wavelengths is indicated by the observation that budding occurs only in the region surrounding the domains prior to monolayer collapse, since monolayer bending on the 1- μm scale is not expected to impact budding [8]. A previous structural study of L-DPPC monolayers at the air/water interface by x-ray reflectivity measured the rms

roughness over a wide range of surface wavelengths (~ 10 nm to $\sim 30\mu\text{m}$) to be $\leq 3.9 \pm 0.1 \text{ \AA}$ for $\pi < 30 \text{ mN/m}$ [20].

How quantitatively reliable is the calibration for determining roughness amplitudes? The roughness is expected to be conformal (displacements of the water-lipid and lipid-air interfaces are highly correlated in space and time) in the purely thermally roughened domains. If the additional roughness in the surrounding region is also conformal, then the intensity calibrations based on the domains should apply exactly to the surrounding region. If the additional roughness in the surrounding is nonconformal to some degree, as might be expected from spatial variations in tilt from the surface normal, for example, then the above intensity calibrations may overestimate the additional amplitude $\Delta\langle\zeta\rangle_{\text{LSM}}$. A rigorous first-order perturbation theory of the angle-resolved light scattering from rough dielectric films at interfaces shows that nonconformal roughness scatters equally as strongly or more strongly than conformal roughness [21]. Our calculations of light scattering into the LSM objective based on the framework of Ref. [21] indicate that $\Delta\langle\zeta\rangle_{\text{LSM}}$ could be overestimated by a factor as large as 2, for the case of light incident at Brewster's angle on a lipid monolayer at the air/water interface with roughness of a few Angstroms.

While the preceding analysis has demonstrated that a slight vertical deformation of the monolayer can quantitatively account for the increased scattering at $\pi = 13 \text{ mN/m}$ in the region surrounding the domains, our LSM data are also consistent with another surface roughness scenario in which bilayer particles rest on the monolayer in the region surrounding the domains. Since bright, individual scattering centers corresponding to bilayer and multibilayer particles (buds) are detected in LSM above $\pi = 20 \text{ mN/m}$, it is possible that the increased scattering above $\pi = 13 \text{ mN/m}$ arises from smaller diameter bilayer buds. To give rise to the spatially uniform increased scattering outside the chiral domains, such small buds would have to be distributed rather evenly outside the domains, and spaced more closely than the $\sim 2.5\text{-}\mu\text{m}$ lateral resolution of the LSM. AFM studies on transferred films cast doubt on the existence of buds below $\pi = 19 \text{ mN/m}$. Several films examined by AFM in air after transfer to mica at $\pi = 15 \text{ mN/m}$ showed no bilayer or multibilayer particles [8,22]. Only a few of the smallest bilayer buds (diameters of 15–40 nm) were detected in one film transferred at $\pi = 19 \text{ mN/m}$, too few to explain the scattering detected with LSM. However, due to the possibility that small buds might reincorporate into the monolayer during or after film transfer, bud formation at $\pi \leq 13 \text{ mN/m}$ cannot be ruled out with confidence.

We now clarify whether the increased scattering at $\pi = 13 \text{ mN/m}$ in the region surrounding the chiral domains might reflect an increase in capillary wave amplitude or the emergence of a permanent roughness. For the surrounding region to allow larger amplitude capillary waves, the surface pressure in the surrounding region would have to be higher than in the domains. With the surface pressure in the domains at $\pi = 13 \text{ mN/m}$, Eq. (1) shows that the pressure in the surrounding would have to rise to $\pi = 39 \text{ mN/m}$ to increase the thermal roughness in the surrounding by 0.4 \AA . Even if we have overestimated the increased roughness amplitude by a factor of 2 and a better estimate is 0.2 \AA , Eq. (1) shows that the pressure in the surrounding would have to rise to π

$= 29 \text{ mN/m}$. In either case, such a large pressure gradient could not be supported by a tilted-condensed monolayer [23]. Therefore, the increased scattering at $\pi = 13 \text{ mN/m}$ in the region surrounding the domains must be caused by static roughness.

IV. CONCLUSIONS

LSM has revealed a previously undetected and unpredicted structural change in condensed L-DPPC monolayers at the air/water interface. These films separate into two topographically distinct regions during compression at $\pi = 13 \text{ mN/m}$, soon after completion of the LE- \rightarrow TC phase transition. For $13 \leq \pi \leq 67.3 \text{ mN/m}$, thermally rough domains with chiral shapes typical for TC domains of L-DPPC are surrounded by a region of increased roughness superimposed on the thermal roughness. Below $\pi = 20 \text{ mN/m}$, the increased roughness outside the chiral domains is due to either a static vertical deformation of the monolayer or small bilayer buds on the monolayer, or a combination of the two. If the increased roughness below $\pi = 20 \text{ mN/m}$ is within the monolayer alone, the scattered intensity from the roughened region corresponds to a deformation amplitude of less than 0.5 \AA within the LSM wavelengths $0.43 \leq \lambda_q \leq 1.52 \mu\text{m}$. Surface roughness in this wavelength range is not laterally resolved with the current LSM lateral resolution of $\sim 2.5 \mu\text{m}$. Above $\pi = 20 \text{ mN/m}$, bilayer and multibilayer buds detectable in both LSM and AFM emerge in the region of increased roughness [8].

We are in the process of improving both the lateral resolution and the sensitivity of the LSM in an attempt to resolve the lateral structure of the roughness in the $\sim 1\text{-}\mu\text{m}$ range of surface wavelengths. With an improved LSM we also hope to resolve possibly earlier stages of static roughness formation between $\pi = 11$ when the edges of TC domains are seen to merge, and $\pi = 13$ when increased scattering is first detected with the current LSM sensitivity. We would like to determine, for example, whether the roughness initiates along narrow domain contact lines and then propagates outward into the domains during compression between $\pi = 11$ and 13 mN/m . Other methods such as synchrotron x-ray scattering at the air/water interface could be employed to investigate the structure of increased roughness in L-DPPC monolayers at smaller length scales.

What might cause the emergence of spatially patterned static roughness in the monolayer? As discussed elsewhere [8], the formation of static roughness at the boundaries between TC domains suggests that its origin lies in packing defects generated as TC domains grow together during the first order LE- \rightarrow TC transition. Future studies are needed to investigate the many questions associated with this model. For instance, why does the increased scattering at $\pi = 13 \text{ mN/m}$ occur over relatively wide regions between chiral-shaped domains rather than along narrow TC domain contact lines? Also, will more precise measurements of the static roughness amplitude show an increase with pressure? Furthermore, with a model of packing defects as the source of this instability in L-DPPC monolayers, the roles of chirality and kinetics are of significant interest.

In addition to presenting the specific findings with L-DPPC monolayers above, this study illustrates the capa-

bilities of LSM in general. Spatially heterogeneous patterns of light scattering can be resolved on microscopic scales at the air/water interface, and the scattered intensities can be quantitatively analyzed. Sensitivity to angstrom level roughness can be achieved. Furthermore, LSM can be combined with other reflection or scattering techniques, including but not limited to BAM, for simultaneous study of films at the air/water interface. The simplicity of LSM and its high sensitivity in an imaging mode suggest the potential to investigate spatial heterogeneity in films at other fluid interfaces

such as, for example, the oil-water interface [24] or freely suspended films [25].

ACKNOWLEDGMENTS

We thank T. A. Germer and G. F. Bertsch for discussions on surface light scattering, and M. Antia and L. Touryan for providing important experimental assistance. This work was supported by NIH Grant Nos. HL3502 and HL60914, NASA Grant No. NAG8-1149, and funds from the Whitaker Foundation and the American Lung Association of Oregon.

-
- [1] D. Langevin, in *Light Scattering by Liquid Surfaces and Complementary Techniques*, edited by D. Langevin (Dekker, New York, 1992), pp. 3–7.
- [2] M. Pluta, *Advanced Light Microscopy* (Elsevier, New York, 1989), Vol. 2, pp. 91–113.
- [3] S. Hénon and J. Meunier, *Rev. Sci. Instrum.* **62**, 936 (1991); D. Hönig and D. Möbius, *J. Phys. Chem.* **95**, 4590 (1991).
- [4] V. M. Kaganer, H. Möhwald, and P. Dutta, *Rev. Mod. Phys.* **71**, 779 (1999).
- [5] L-DPPC does not reach the untilted state prior to collapse.
- [6] M. M. Lipp *et al.*, *Phys. Rev. Lett.* **81**, 1650 (1998).
- [7] A. Saint-Jalmes and F. Gallet, *Eur. Phys. J* **2**, 489 (1998); C. Fradin *et al.*, *Physica B* **248**, 310 (1998).
- [8] W. R. Schief, L. Touryan, S. B. Hall, and V. Vogel, *J. Phys. Chem. B* **104**, 7388 (2000).
- [9] H. McConnell, *Annu. Rev. Phys. Chem.* **41**, 441 (1990).
- [10] C. W. McConlogue and T. K. Vanderlick, *Langmuir* **13**, 7158 (1997).
- [11] At short length scales ($\lambda_q \sim 10$ nm), recent evidence indicates that bare fluid interfaces are rougher than predicted by the capillary wave model [C. Fradin *et al.*, *Nature (London)* **403**, 871 (2000)]. Also at small scales, the bending rigidity of a monolayer reduces the roughness of a fluid interface [C. Fradin *et al.*, *Physica B* **248**, 310 (1998); C. Gourier *et al.*, *Phys. Rev. Lett.* **78**, 3157 (1997)]. At large length scales ($\lambda_q \sim 2\pi[\gamma/(\rho_{\text{water}}-\rho_{\text{air}})g]^{1/2} \sim \text{cm}$) gravity limits the roughness.
- [12] Each mode acts as a sinusoidal diffraction grating, and these only produce first order diffraction. The range of surface wavelengths which scatter into the LSM objective ($NA=0.45$) can therefore be calculated from the n th order grating equation in the plane of incidence: $n\lambda_{\text{laser}}/\lambda_q = \sin\theta_{\text{scat}} - \sin\theta_{\text{incident}}$ [J. Lekner, *Theory of Reflection* (Martinus Nijhoff, Dordrecht, 1987), p. 207.] In this work, $n=-1$, $\theta_{\text{incident}} \approx 53.1^\circ$, and θ_{scat} is measured from the interface normal and defined to be positive in the direction of specular reflection.
- [13] At each point in a LSM image, the diffracted light is collected from different modes present within the corresponding region of the interface. The LSM image intensity is therefore proportional to the square of the sum of the complex far-field amplitudes scattered from these modes: $I_{\text{LSM}} \propto |\sum A_q|^2$, where the sum is over the modes with wavelength in the range $0.43 \leq \lambda_q \leq 1.52 \mu\text{m}$. For $\zeta_q/\lambda_{\text{laser}} \ll 1$, $A_q \propto \langle \zeta_q \rangle$ [J. M. Elson, *J. Opt. Soc. Am. A* **12**, 729 (1995)]. Therefore, since $\langle \zeta_q^2 \rangle \propto 1/\gamma$ from capillary wave theory, $I_{\text{LSM}} \propto 1/\gamma$.
- [14] At higher pressures, intense scattering from the high density of point scatterers necessitated a reduction in camera gain, so quantitative intensity analysis was hindered.
- [15] V. T. Moy, D. J. Keller, H. E. Gaub, and H. M. McConnell, *J. Phys. Chem.* **90**, 3198 (1986).
- [16] G. Weidemann and D. Vollhardt, *Colloids Surf., A* **100**, 187 (1995).
- [17] LSM detects no scattering from the tilt azimuth boundaries detected with BAM in the TC phase of monolayers of the following compounds: dimyristyl phosphatidylethanolamine, dipalmitoyl phosphatidylglycerol, myristic acid, pentadecanoic acid, and arachidic acid.
- [18] *Light Scattering by Liquid Surfaces and Complementary Techniques* (Ref. [1]), pp. 28–30.
- [19] R. Loudon, in *Surface Excitations*, edited by V. M. Agranovich and R. Loudon (North-Holland, Amsterdam, 1984), pp. 593–596. We perform the integration of Eq. (10), p. 596, from q_{min} to q_{max} rather than from 0 to Q_m .
- [20] J. Daillant *et al.*, *J. Phys. II* **1**, 149 (1991).
- [21] J. M. Elson, *J. Opt. Soc. Am. A* **12**, 729 (1995).
- [22] The only topographic feature detected by AFM on films transferred below $\pi=20$ mN/m was a weblike network of linear depressions approximately 3 Å deep and <15 nm wide, covering the entire monolayer (detected from $\pi=15$ to 40 mN/m). This network was similar in morphology to the fluorescent networks found by near-field optical scanning microscopy on fluorescently labeled DPPC monolayers transferred onto mica [J. Hwang, *et al.*, *Science* **270**, 610 (1995)]. The network might be related to the source of the increased scattering detected by LSM at the air/water interface at $\pi \geq 13$ mN/m outside the dark domains. However, AFM detected no network-free regions on transferred films that might correspond to the dark domains at the air/water interface, while AFM did show bud-free regions suggestive of such domains in films transferred above $\pi=20$ mN/m. Hence the network might also be an artifact of the transfer process and/or subsequent relaxation processes of the film in ambient air on mica.
- [23] K. Miyano, *Langmuir* **6**, 125 (1990).
- [24] L. T. Lee, D. Langevin, and B. Farnoux, *Phys. Rev. Lett.* **67**, 2678 (1991); R. Teppner, M. Harke, and H. Motschmann, *Rev. Sci. Instrum.* **68**, 4177 (1997).
- [25] C.-M. Chen and F. C. MacKintosh, *Phys. Rev. E* **53**, 4933 (1996); A. Fera, B. I. Ostrovskii, D. Santenac, I. Samoilenko, and W. H. de Jeu, *ibid.* **60**, R5033 (1999).